INT. J. NUM. METH. HEAT FLUID FLOW, VOL. 4, 483–496 (1994)

TURBULENT NATURAL CONVECTION IN A SIDEWALL-HEATED CAVITY USING A TWO-EQUATION MODEL OF TEMPERATURE

TORU FUSEGI

Energy Technology Research Institute, Tokyo Gas Co, Ltd, 1-16-25 Shibaura, Minato, Tokyo 105, Japan

ABSTRACT

A calculation procedure for turbulent natural convection in enclosures is described. A two-equation model based on the eddy diffusivity concept for the temperature field possessing a form similar to the k–ε model of flow is incorporated, thus, extending the applicability of the eddy diffusivity models by removing constraints of the Reynolds analogy between momentum and thermal transport processes. As a test problem, natural convection in a square cavity subjected to differential side-wall heating is analysed. The vertical walls are divided into isothermal and constant heat-flux surfaces and heated non-uniformly. At $Ra = 10^{10}$ and for an air-filled cavity ($Pr = 0.71$), variations of heating patterns are found to significantly alter the field characteristics. Numerical predictions demonstrate dissimilar features of the velocity and temperature fluctuations.

KEY WORDS Turbulent heat transfer One-point closure for turbulent heat flux Numerical methods Natural convection in an enclosure

NOMENCLATURE

c_1, c_2, h_1, h_2	locations of the heating elements (see *Figure 1*), $(c_1^*, c_2^*, h_1^*, h_2^*)/L_0$	Nu	Nusselt number, $Nu \equiv -\partial T/\partial x$ (local Nu) and $\overline{Nu} \equiv \int_1^0 Nu\, dy$ (average Nu)
c_p	specific heat at constant pressure, c_p^*/c_{p0}	Pr	molecular Prandtl number, $c_{p0}\mu_0/\lambda_0$
$C_\mu, C_{\varepsilon 1}, C_{\varepsilon 2}$	turbulence model constants for the velocity field	Pr_t	turbulent Prandtl number, $c_{p0}\mu_t^*/\lambda_t^*$
$C_\lambda, C_{D1}, C_{D2}, C_{P1}, C_{P2}$	turbulence model constants for the temperature field	$Pr_k, Pr_\varepsilon, Pr_q, Pr_G$	Prandtl numbers for k, ε, q and G equations, respectively
g	gravitational acceleration, g^*/g_0	q	temperature variance, $q^*/(T_H - T_C)^2$ where $q^* \equiv \overline{T^{*\prime 2}}$
G	variable, $G^* L_0^2/(T_H - T_C)^2$ where $G^* = \gamma^*/(\lambda^*/\rho^* c_p^*)$	Q	heat flux, $Q^* L_0/\mu_0 c_{p0} \times (T_H - T_C) Ra^{1/4}$
k	turbulent kinetic energy, $k^*(\rho_0 L_0/\mu_0 Ra^{1/4})^2$ where $k^* \equiv \overline{u_i^{*\prime} u_i^{*\prime}}/2$	Ra	Rayleigh number, $g_0\beta_0 c_{p0}\rho_0^2 L_0^3 (T_H - T_C)/\mu_0\lambda_0$
L_0	reference length (enclosure width) [m]	t	time, $t^*(\mu_0 Ra^{1/4}/\rho_0 L_0^2)$
		T	time-averaged tempera-

0961–5539/94/060483–14$2.00
© 1994 Pineridge Press Ltd

Received March 1993
Revised November 1993

© Emerald Backfiles 2007

ture, $(T^* - T_C)/(T_H - T_C)$

T_C, T_H temperatures of the cooled and heated isothermal surfaces, respectively [K]

u, v time-averaged velocity components in the x and y directions, $(u^*, v^*)\rho_0 L_0/\mu_0 Ra^{1/4}$ ($\rho^* u^* \equiv \partial\psi^*/\partial y^*$ and $\rho^* v^* \equiv -\partial\psi^*/\partial x^*$)

x, y Cartesian coordinates, $(x^*, y^*)/L_0$

ε dissipation rate of k, $\varepsilon^*(\rho_0^3 L_0^4/\mu_0^3 Ra^{3/4})$ where $\varepsilon^* = (\mu^*/\rho^*) \times \overline{(\partial u_i^{*\prime}/\partial x_j^*)(\partial u_j^{*\prime}/\partial x_i^*)}$

λ, λ_t molecular and eddy thermal conductivities, $(\lambda^*, \lambda_t^*)/\lambda_0$

μ, μ_t molecular and eddy viscosities, $(\mu^*, \mu_t^*)/\mu_0$

ρ density, ρ^*/ρ_0

ψ stream function, $\psi^*\rho_0/\mu_0 Ra^{1/4}$

ω vorticity, $\omega^*\rho_0 L_0^2/\mu_0 Ra^{1/4}$

Greek symbols

β thermal expansion coefficient, β^*/β_0

γ dissipation rate of $q/2$, $\gamma^*(\rho_0 c_{p0}/\lambda_0)L_0^2/(T_H - T_C)^2$ where $\gamma^* = (\lambda^*/\rho^* c_p^*) \times \overline{(\partial T^{*\prime}/\partial x_j^*)(\partial T^{*\prime}/\partial x_j^*)}$

Superscripts

$'$ fluctuation component

$*$ dimensional quantity

$—$ average value

Subscript

0 reference value

INTRODUCTION

Turbulent natural convection in confined space is commonly encountered in a variety of thermal engineering systems. They include air conditioning in rooms, electronic device cooling, crystal growth in liquids, solar energy collectors, to name but a few. Due to the importance of accurately predicting flow and heat transfer characteristics of turbulent natural convection in enclosures, numerical and experimental investigations on the subject have attracted much research attention. In the past computational work, various classes of turbulence models have been employed, e.g., two-equation k–ε eddy viscosity models[1–4], an algebraic Reynolds stress model[3] and direct numerical simulation methods[5,6]. These investigations considered a channel of rectangular cross-section having differentially-heated side walls, the well-known 'double-glazing problem'. In a number of applications, however, the thermal boundary conditions are not necessarily uniform over the entire length of walls, owing to the presence of localized wall-mounted panel heaters and a computer chip, to cite examples.

Prior computational studies for these situations reported in the heat transfer literature are rather scarce. Ozoe *et al.*[7] examined turbulent natural convection in a cubic box with a partially-cooled side wall and the heated floor. Placing in mind specific applications to air conditioning in a room, Lankhorst and Hoogendoorn[8] analysed natural convective flow patterns in a room equipped with a side-wall-mounted modelled radiator. These computations are performed by using k–ε models modified for buoyancy induced flows. Turbulent heat transfer was dealt with by assuming the Reynolds analogy between momentum and thermal transport; hence, the eddy thermal conductivity λ_t was calculated from the eddy viscosity μ_t, which was directly evaluated by the k–ε model, as $\lambda_t = \mu_t c_p/Pr_t$, Pr_t being the turbulent Prandtl number. The analysis was further simplified by setting a constant value to Pr_t.

Strict validity of such an approach is restricted to the cases in which hydrodynamic and thermal boundary-layers developing near the cavity walls are similar. In other words, the thermal boundary condition for a solid no-slip wall must be uniform over the entire length. To provide

© Emerald Backfiles 2007

more flexibility for applicable thermal boundary conditions, a plausible method is conceived in which the eddy conductivity is determined independently using turbulent heat-transfer properties in the field. An obvious advantage of such a calculation procedure is that the temperature fluctuations of the field are directly assessed; hence, more reliable information concerning thermal characteristics of the system under investigation is acquired. Several two-equation models for thermal transport processes possessing a form similar to the k–ε flow model have been proposed[9–14].

Recall that, in the eddy viscosity model, μ_t is taken to be proportional to the product of the turbulent velocity scale ($k^{1/2}$) and the characteristic length scale, for which the eddy length scale ($k^{3/2}/\varepsilon$) is employed. Based on a similar argument, the eddy thermal conductivity λ_t is equated to the product of the turbulent velocity, an appropriate length scale for measuring temperature fluctuations, and a proportionality constant. As the length scale of question, a mixing time-scale, $k^{1/2}(k/\varepsilon)^l(q/\gamma)^m$, is selected, where q and γ respectively denote the temperature variance and its rate of dissipation as defined in the Nomenclature. This quantity can properly blend the time scales for the velocity field (k/ε) and for the thermal field (q/γ); hence, λ_t may be represented as:

$$\lambda_t^* = C_\lambda \rho^* c_p^* k^* (k^*/\varepsilon^*)^l (q^*/\gamma^*)^m \tag{1}$$

It can be seen that the sum of l and m must be equal to unity to maintain the dimensional consistency. Possible combinations of these exponents are thought to be $l = m = 0.5$[11], $l = -1$ and $m = 2$[12,15], or $l = 0$ and $m = 1$[13]. No standard values for l and m providing general applicability appear to exist. Note that the above expression reduces to the conventional constant-Pr_t method by choosing $l = 1$ and $m = 0$.

Computations incorporating these two-equation models for temperature were conducted for the thermal entrance-region of developed pipe flows[11], forced convection in a flat-plate boundary layer accompanying sudden changes in the thermal boundary conditions[12,15] and for free stream turbulence[13].

The present paper examines turbulent natural convection in a two-dimensional square cavity, which is heated differentially and non-uniformly at the side walls. The schematic diagram of the geometry under consideration is shown in *Figure 1*. The fluid ($Pr = 0.71$) is bounded by solid no-slip walls. The wide walls located at $x^* = 0$ and L_0 are partially heated to prescribed temperatures. Constant heat fluxes are imposed over the remaining portions of the vertical walls. The horizontal walls ($y^* = 0$ and L_0) are presumed to be thermally insulated. This simple geometry is chosen to test the applicability of the two-equation models for momentum and thermal transport processes for natural convection in enclosures. The exponents appearing in (1) are set to $l = 0$ and $m = 1$ as the simplest expressions and for consideration of numerical stability. The problem to be investigated is regarded as a basic model for many practical applications, for instance, air conditioning in a building. The present investigation is conducted

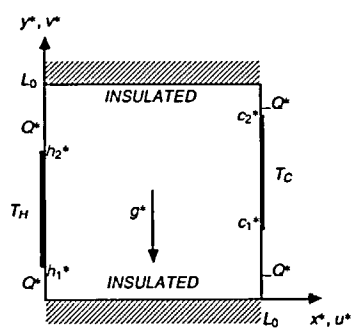

Figure 1 The flow geometry of interest

© Emerald Backfiles 2007

as a first stage towards developing an improved turbulent flow calculation procedure for natural convection in confined flows utilizing the eddy diffusivity model. Salient features of the flow and heat transfer patterns inside the cavity are delineated, with an emphasis on turbulence characteristics. The effects of heat conduction between the isothermal elements and uniform heat-flux surfaces are also accounted for in the computations.

MATHEMATICAL MODEL

Two-dimensional incompressible mean flow and heat transfer are assumed. The Boussinesq approximation is invoked for variations of the physical properties of fluid. The Reynolds-averaged governing equations describe the conservation of mass, momentum and energy. The stream function–vorticity formulation is selected for the present two-dimensional numerical study. Invoking the k–ε model and the two-equation model of temperature described in the previous section, four additional equations are included in the governing equation system: they are the equations of the turbulent kinetic energy k; its rate of dissipation ε; temperature variance q; and the dissipation rate of $q/2$, γ. In the present analysis, the last quantity is replaced by G, which is defined as $G = \gamma/a$, where a is the (molecular) thermal diffusivity of fluid. All of these equations can be cast into the general expression:

$$\alpha\left\{\frac{\partial\phi}{\partial t} + \frac{\partial}{\partial x}(u\phi) + \frac{\partial}{\partial y}(v\phi)\right\} = \frac{\partial}{\partial x}\left(\Gamma\frac{\partial\phi}{\partial x}\right) + \frac{\partial}{\partial y}\left(\Gamma\frac{\partial\phi}{\partial y}\right) + S(x, y) \tag{2}$$

where α denotes a constant (either 0 or 1), ϕ is any dependent variable (ψ, ω, T, k, ε, q or G), Γ represents an exchange coefficient and S stands for the source term. The complete set of the governing equations is found in the Appendix. The non-dimensionalization of the physical quantities are indicated in the Nomenclature.

The governing equations system is solved subject to appropriate boundary conditions. On the no-slip walls, the stream function ψ is set equal to 0 and the vorticity at the wall is computed from the definition: $\omega = (\partial u/\partial y) - (\partial v/\partial x)$. The following thermal and turbulence boundary conditions are assigned:

$$\begin{cases} T = 1\,(h_1 \leqslant y \leqslant h_2), \text{otherwise} \; -Ra^{-1/4}Pr^{-1}\left.\dfrac{\partial T}{\partial x}\right|_{\text{wall}} = Q_{\text{wall}} \quad \text{at } x = 0 \\ T = 0\,(c_1 \leqslant y \leqslant c_2), \text{otherwise} \; Ra^{-1/4}Pr^{-1}\left.\dfrac{\partial T}{\partial x}\right|_{\text{wall}} = -Q_{\text{wall}} \quad \text{at } x = 1 \end{cases} \tag{3}$$

$$\frac{\partial T}{\partial y} = 0 \quad \text{at } y = 0, 1 \tag{4}$$

$$\left.\begin{array}{l} k = 0, \varepsilon = 2Ra^{-1/4}\left.\left(\dfrac{\partial\sqrt{k}}{\partial n}\right)^2\right|_{\text{wall}} \\ q = 0 \text{ if } T_{\text{wall}} = \text{constant}, \dfrac{\partial q}{\partial n} = 0 \text{ if } Q_{\text{wall}} = \text{constant} \\ G = \left.\left(\dfrac{\partial\sqrt{q}}{\partial n}\right)^2\right|_{\text{wall}} \end{array}\right\} \text{at } x = 0, 1 \text{ and } y = 0, 1 \tag{5}$$

where n denotes the coordinate normal to the wall. The turbulence field is solved all the way to the wall, without implementing the so-called 'wall functions'.

© Emerald Backfiles 2007

SOLUTION METHOD

A finite difference solution method is adopted. Prior to the solution procedure, the governing equations written in the physical coordinate (x–y) system, together with the boundary conditions, are transformed into a computational coordinate (ξ–η) system. In the latter, equidistant, orthogonal calculation meshes are distributed.

Partial derivatives in these two coordinate systems are related as:

$$\frac{\partial \phi}{\partial x} = \frac{1}{J}\left[\frac{\partial}{\partial \xi}(J\xi_x \phi) + \frac{\partial}{\partial \eta}(J\eta_x \phi)\right], \qquad \frac{\partial \phi}{\partial y} = \frac{1}{J}\left[\frac{\partial}{\partial \xi}(J\xi_y \phi) + \frac{\partial}{\partial \eta}(J\eta_y \phi)\right] \tag{6}$$

where J is the Jacobian of transformation defined as $J = x_\xi y_\eta - x_\eta y_\xi$ and a_b (ξ_x, etc.) stands for $\partial a/\partial b$. The contravariant velocity components, U ($\equiv \xi_x u + \xi_y v$) and V ($\equiv \eta_x u + \eta_y v$), are introduced to derive a transformed general governing-equation in a form similar to the original:

$$\alpha\left\{\frac{\partial \phi}{\partial t} + \frac{1}{J}\frac{\partial}{\partial \xi}(JU\phi) + \frac{1}{J}\frac{\partial}{\partial \eta}(JV\phi)\right\} = \frac{1}{J}\frac{\partial}{\partial \xi}\left[\Gamma J\left(a_1 \frac{\partial \phi}{\partial \xi} + a_2 \frac{\partial \phi}{\partial \eta}\right)\right] + \frac{1}{J}\frac{\partial}{\partial \eta}\left[\Gamma J\left(a_2 \frac{\partial \phi}{\partial \xi} + a_3 \frac{\partial \phi}{\partial \eta}\right)\right] + S(\xi, \eta) \tag{7}$$

where $a_1 = \xi_x^2 + \xi_y^2$, $a_2 = \xi_x \eta_x + \xi_y \eta_y$ and $a_3 = \eta_x^2 + \eta_y^2$. This mathematical transformation is straightforward but rather tedious. Resulting equations to be solved in the computational space are lengthy and, hence, they are not presented. Note that in the square cavity problem of the present interest, finite difference grids in the physical space are also orthogonal; therefore, the cross-derivatives ξ_y and η_x vanish, leading to a considerable simplification for the transformed equations.

Finite difference equations are obtained by ways of control-volume based technique[16]. This ensures the conservation of physical quantities in every computational cell, i.e. control volume. The convection terms in the vorticity-transport and energy equations are treated by the QUICK scheme[17] in order to reduce the numerical diffusion. For the reason of numerical stability, the hybrid scheme[16] is applied to the turbulence equations (for k, ε, q and G). The second derivatives are discretized using the central differencing. One-sided difference formulae with second-order accuracy are adopted to compute the vorticity at the wall from the velocity components. The Euler backward differencing is utilized for the time derivatives. Finite difference non-linear algebraic equations are solved iteratively using the strongly implicit procedure[18].

Convergence at each time step is declared when changes in all the dependent variables between two consecutive iterations fall below a prescribed convergence criterion:

$$|\phi_{i,j}^n - \phi_{i,j}^{n-1}|/|\phi^n|_{\max} \leqslant 10^{-4} \quad \text{for all grid points } (i,j) \tag{8}$$

where n and $n-1$ are iteration levels and $|\phi^n|_{\max}$ denotes an absolute maximum of variable ϕ at the nth iteration.

The whole cavity interior is considered as the full computational field. The total number of meshes is 42×43. Grid dependence of solutions is discussed in a later section. Variable grids are used in the physical space, for which meshes are dense in the vicinity of the walls, in order to adequately resolve the near-wall boundary layers. Use is made of a non-uniform grid generation scheme described in Anderson *et al.*[19] to locate three to four nodes between the wall and the peak velocity of the boundary layer. Approximately ten meshes are distributed inside the boundary layer. To validate the developed computer code, results for the double-glazing problem (isothermal side walls) are compared with laminar-flow benchmark solutions for $Ra \leqslant 10^8$ proposed by de Vahl Davis[20] and Le Quére[21]. The present numerical predictions are found to agree within 1% difference of the reference data.

© Emerald Backfiles 2007

RESULTS AND DISCUSSION

Steady state solutions at $Ra = 10^{10}$ are obtained after time marching of approximately 50,000 time steps with a time increment of 10^{-5} starting from a lower Ra laminar-flow result, which is used as an initial guess. This is regarded to be a very slow convergence process, due partly to substantially high grid aspect-ratios associated with the use of the low-Re type turbulence model. In this section, illustrative flow features and heat transfer characteristics inside the cavity are scrutinized for $Ra = 10^{10}$ and $Q_{wall} = 0.3$. The locations of the isothermal heating/cooling elements are varied systematically.

First, computations were conducted for the case in which $c_1 = h_1 = 0$ and $c_2 = h_2 = 1$, i.e., the entire side walls are isothermally heated or cooled. Due to lack of reliable experimental data for the present problem, this serves as a verification case for the computational model since prior numerical predictions are available in the literature[1,3–5]. For these calculations, various high Reynolds number versions of the k–ε model were employed, with or without wall functions for near-wall treatment. An exception is a direct numerical simulation by Paolucci who integrated unsteady Navier–Stokes equations without modelling turbulence explicitly. In solving the Reynolds-averaged temperature equation, all the studies using k–ε models assumed the turbulent Prandtl number Pr_t to be a constant value at around unity.

In the present investigation employing the k–ε and q–G model, runs are also made by using a low Re k–ε model. The computed results for these two models are respectively referred to as model 1 and model 2 in *Table 1*. For model 2, the q and G equations are not solved; λ_t contained in the energy and k equations is replaced by $\mu_t Pr/Pr_t$, with $Pr_t = 0.9$.

Representative quantities of the cavity flow are summarized in *Table 1*, together with the existing results in the literature. In the present predictions listed in the second and third columns, when the entire side walls are isothermal, the peak velocity in the boundary layer near the heated side wall, the local and overall Nusselt numbers and the maximum eddy viscosity differ only slightly. On the other hand, the maximum value of the eddy thermal conductivity independently calculated by the two-equation model of temperature (model 1) attains a higher value than the model 2 prediction estimated from the maximum eddy–viscosity and a constant Pr_t. For the

Table 1 Comparison of representative physical quantities for the case of the isothermal side walls

	Present results		Markatos & Pericleous (k–ε model)[1]	Silva & Emery (k–ε)[3]	Lankhorst (k–ε)[4]	Paolucci (DNS)[5]
	Model 1[a]	Model 2[b]				
v_{max} at $(x, 0.5)$						
v_{max} =	75.45	79.66	75.23	83.2	67.06	95.8
x =	0.00365	0.00365	0.0055	0.004	—	0.00458
$\overline{Nu}$ at $x = 0$						
$\overline{Nu}$ =	96.04	107.7	156.9	127.2	140.7	99.54
Nu_{max} at $(0, y)$						
Nu_{max} =	465.6	460.1	361.47	428.6	—	—
y =	0.00190	0.00190	0.001	0.00125		
$\mu_{t,max}$ at (x, y)						
$\mu_{t,max}$ =	16.47	16.87	—	23.6	28.8	—
(x, y) =	(0.9739, 0.1357)	(0.9755, 0.3601)	—	(0.97, 0.295)	—	
$\lambda_{t,max}$ at (x, y)						
$\lambda_{t,max}$ =	56.59	[13.3][2]	—	—	—	—
(x, y) =	(0.0179, 0.8395)					

[a] Model 1 refers to the two-equation models for momentum and thermal transport, and Model 2 stands for the low Re k–ε model with $Pr_t = 0.9$.
[b] $\lambda_{t,max} = \mu_{t,max} Pr/Pr_t$.

© Emerald Backfiles 2007

isothermal side walls, spatial distributions of turbulence quantities for heat (q, G and λ_t) are found to be very similar to those for flow, i.e., k, ε and μ_t (not shown).

The present computed results using the low Reynolds number form of the turbulence equations are compared with those in the previously reported investigations. For the peak velocities, the calculated values employing the eddy–viscosity turbulence models are consistently lower than the DNS data by about 20%. An apparent difference arises among the predictions for the heat transfer rate at the side wall. The past investigations overpredicted the average Nusselt number, while the present results are much closer to the DNS data. This may be a reflection of considerably high eddy viscosities computed by the high Re k–ε models. Overall, the present results for the two-equation models of flow and heat transfer are consistent with the k–ε model predictions for the case of the isothermal side walls.

Partially isothermal side walls

Variations of the flow patterns due to the changes in the locations of the isothermal elements are investigated in this subsection. The length of the partial heater/cooler is held at 0.5; one-half the side wall is maintained at constant temperatures, while a uniform heat flux of $|Q_{wall}| = 0.3$ is imposed to the remaining portions of the vertical side walls. The following three different heater locations are considered: $h_1 = 0$ and $c_1 = 0.5$ (hereafter referred to as Case A), $h_1 = c_1 = 0.5$ (Case B), and $h_1 = 0.5$ and $c_1 = 0$ (Case C). The computed field values for these cases are compiled in *Table 2*. Owing to the field symmetry in Cases A and C, the absolute values of the maximum and minimum velocities are identical within the accuracy of numerical errors. In contrast, the magnitude of u_{max} and u_{min} for Case B differs appreciably due to the asymmetric heating pattern. The turbulence quantities ($\lambda_{t,max}$ and $\mu_{t,max}$) for Case C are seen to be substantially lower than those of Case A. Note also that the peak values of the vertical velocity (v) differ significantly for these two cases. These differences are attributable to the variations in the heating patterns.

The spatial distributions of the turbulent kinetic energy k and the temperature variance q are inspected for Cases A and B with the aid of isovalue contour maps, as illustrated in *Figures 2* and *3*. In Case A (*Figure 2*), only upper-left portions of the entire fields are displayed due to the centro-symmetry of the fields. The regions of high turbulent energies for momentum and heat are seen to be located near the upper-left corner at which the developed hydrodynamic

Table 2 Characteristic field variables for different locations of the isothermal elements (Model 1 predictions, unless otherwise indicated)

	Case A	Case B	Case B (Model 2)	Case C
u_{max}	15.56	24.7	20.22	31.59
(x, y)	(0.0128, 0.9976)	(0.0245, 0.9947)	(0.0245, 0.9947)	(0.0330, 0.9947)
u_{min}	−15.38	−12.11	−10.9	−31.72
(x, y)	(0.9872, 0.00238)	(0.9872, 0.00238)	(0.9911, 0.00238)	(0.9670, 0.00531)
v_{max}	99.24	69.48	71.37	56.04
(x, y)	(0.00365, 0.447)	(0.00365, 0.75)	(0.00365, 0.75)	(0.00365, 0.6286)
v_{min}	−99.10	−73.37	−71.0	−56.34
(x, y)	(0.9964, 0.553)	(0.9964, 0.75)	(0.9964, 0.75)	(0.9964, 0.371)
$\mu_{t,max}$	11.06	8.728	8.165	2.30
(x, y)	(0.9755, 0.25)	(0.9821, 0.5842)	(0.0179, 0.8147)	(0.9560, 0.0317)
$\lambda_{t,max}$	33.17	26.75	—	7.25
(x, y)	(0.9821, 0.0317)	(0.0179, 0.9474)		(0.9821, 0.0842)
$\overline{Nu}$	75.9	122	121	182

© Emerald Backfiles 2007

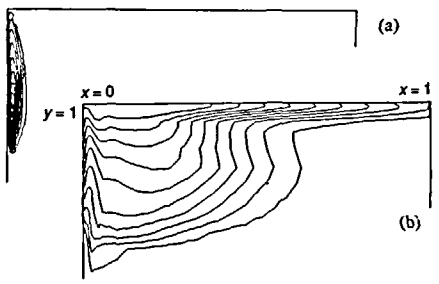

Figure 2 Distributions of k and q (case A): (a) k, (b) q [increments of the isolevel contours for $k/|v_{max}|^2 = 6.51 \times 10^{-3}$ and for $q = 3.60 \times 10^{-3}$; coordinate locations (x, y) for $k_{max} = (0.0128, 0.685)$ and $q_{max} = (0.0593, 0.9947)$]

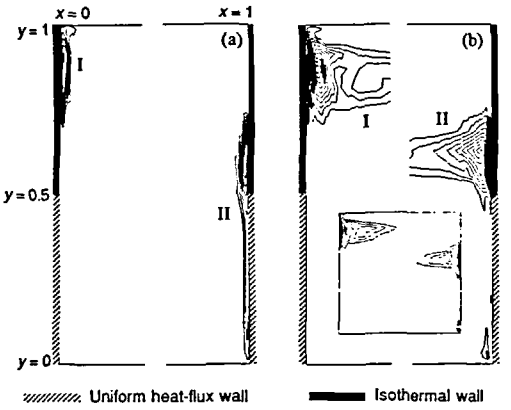

Figure 3 Distributions of k and q (case B): (a) k, (b) q [increments of the isolevel contours for $k/|v_{max}|^2 = 7.70 \times 10^{-3}$ and for $q = 2.71 \times 10^{-5}$; $k^{I}_{max} = 7.70 \times 10^{-2}$ at $(x, y) = (0.0891, 0.815)$, $k^{II}_{max} = 7.52 \times 10^{-2}$ at $(0.9872, 0.584)$, $q^{I}_{max} = 2.71 \times 10^{-3}$ at $(0.033, 0.871)$, and $q^{II}_{max} = 2.54 \times 10^{-3}$ at $(0.9755, 0.629)$, where I and II refer to the contour line groups marked in the Figure]

and thermal boundary-layers impinge. Although the high turbulent kinetic energy is confined to the side-wall boundary layer, the areas of appreciably high temperature variances spread to a much larger portion of the flow field. This distinctively different behaviour of the velocity and temperature fluctuations may be attributable to the dissimilar boundary conditions at the horizontal walls (see (5)). At the no-slip wall, k is identically zero; however, the *flux* of q is set to zero, which allows the penetration of appreciable temperature fluctuations into the central region of the flow field. Under the present thermal boundary-conditions, normalized turbulence intensities measured by $k_{max}/|v_{max}|^2$ and q_{max} are seen to be comparable.

Figure 3 represents computed results for Case B in which asymmetric heating is applied to the side walls. The flow fields in the close proximity of the wide walls are displayed to highlight detailed field structure. It should be recognized that considerable turbulent energies are contained in the near-wall regions covering much of the cooled side wall ($x = 1$). From the upper-right corner ($x = y = 1$) down to the cavity mid-height ($y = 0.5$), fluid is cooled by an isothermal element, followed by a uniform heat flux in $0 \leqslant y \leqslant 0.5$. High temperature variances are detected in the field near the mid-height where the thermal boundary conditions undergo an abrupt change. In this case, the turbulence intensities for the temperature field are found to be overall one order of magnitude lower than those of the flow field.

The velocity and temperature profiles near the side walls for Case B are shown in *Figures 4* and *5*. As depicted in *Figure 4a*, in the vicinity of the heated wall ($x = 0$), the vertical velocity is rather uniform in the lower part of the wall ($0 \leqslant y \leqslant 0.5$), to which a constant heat flux is imposed. Close to the isothermal hot plate above it, the flow is seen to be accelerated considerably. At the cooled side wall ($x = 1$), the overall flow patterns are similar to those near the heated wall previously inspected. However, in this case, steep velocity gradients prevail over the areas covering from the cavity mid-height down to the region near the floor ($y = 0$). These sustain high turbulence over the constant heat-flux wall; see also *Figure 3*. It is interesting to note that mostly antisymmetric temperature distributions are observed near the side walls, as illustrated in *Figure 5*. Hence, the heat transfer rate to the isothermal portions of the side walls vary in an almost antisymmetric fashion, which is also evident in *Figure 7* (the curves corresponding to

© Emerald Backfiles 2007

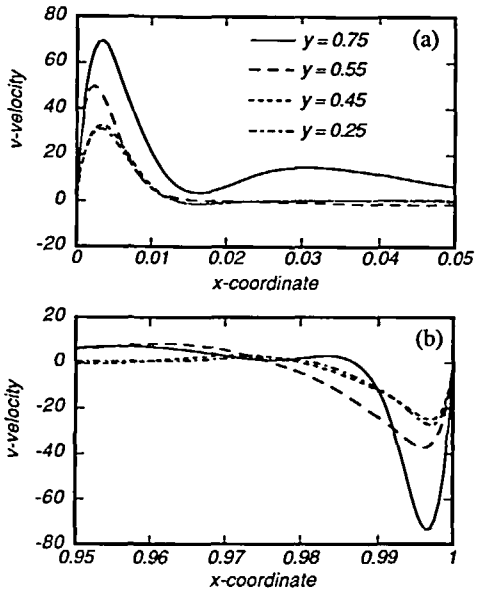

Figure 4 Vertical velocity profiles at various y locations near the side walls (case B): (a) near the heated wall ($x = 0$), (b) near the cooled wall ($x = 1$)

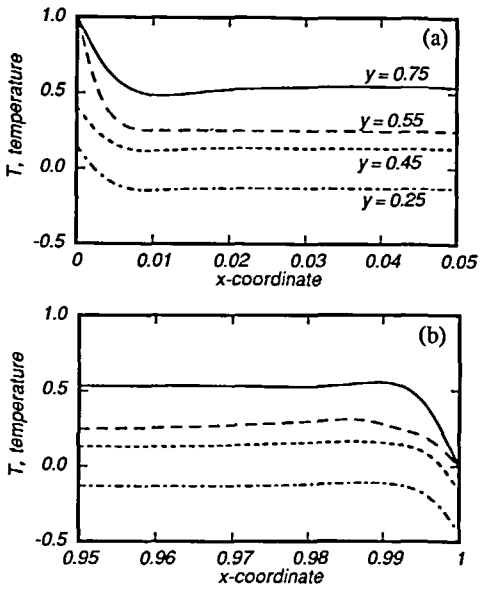

Figure 5 Temperature distributions at different height near the side walls (case B): (a) near the heated wall ($x = 0$), (b) near the cooled wall ($x = 1$)

$dl = 0$). Note that the negative temperature regions appear at $y = 0.25$, indicating that the fluid temperature near the constant heat-flux wall ($y < 0.5$) is lower than the temperature of the cooled isothermal-wall ($T = 0$).

Turbulence intensities in the near-wall boundary layer are closely examined next for Case B. *Figure 6* presents profiles of the eddy viscosity, μ_t, and the thermal conductivity, λ_t, together with the turbulent Prandtl number, Pr_t, at the three different elevations. Recall that the boundary layer develops downward along the cooled wall ($x = 1$); consequently, μ_t and λ_t at $y = 0.25$ are considerably reduced compared to those at around $y = 0.5$. It should be noted that the profiles of the eddy conductivity change remarkably within a short distance across the cavity mid-height at which the thermal boundary conditions are suddenly altered. In contrast, the shape of the μ_t profiles remains almost identical in this region. Computed values of Pr_t are depicted in *Figure 6c*. They undergo noticeable variations inside the boundary layer. In the immediate vicinity of the wall, both μ_t and λ_t rapidly diminish to zero. Consequently, Pr_t is indeterminable there. A similar trend occurs in the regions close to the outer edges of the boundary layer. This precludes a precise assessment of the distribution of Pr_t in the flow field. This, however, is not a drawback of the present method, since Pr_t does not appear explicitly in the entire calculation procedure.

The distributions of the velocity and temperature at the cavity mid-height ($y = 0.5$), predicted by employing Model 1 (k–ε and q–G model) and Model 2 (k–ε), are displayed in *Figure 7* for Case B. The boundary-layer profiles are similar in both cases; however, deviations become apparent in the regions away from the side wall. The computed maxima and minima of the representative field variables for both models are presented in *Table 2*. They do not differ substantially, only by about 5%, since their locations are inside the boundary layers.

Effects of conduction between the isothermal and constant heat-flux elements

So far, conduction between an isothermal element and an adjacent uniform heat flux surface of the side wall has been neglected in the analysis. However, this is a highly idealized situation,

© Emerald Backfiles 2007

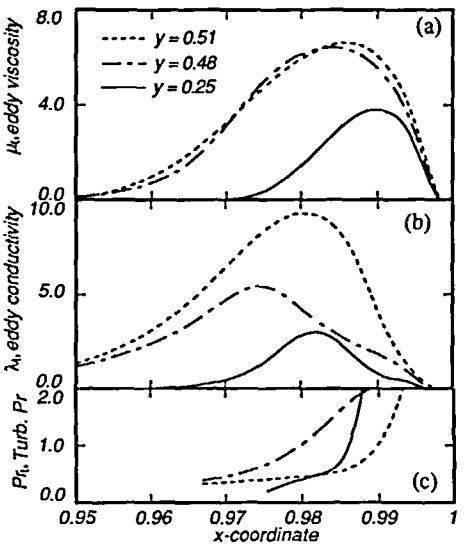

Figure 6 Variations of (a) the eddy viscosity, (b) eddy thermal conductivity, and (c) turbulent Prandtl number near the cooled wall at $x = 1$ (case B)

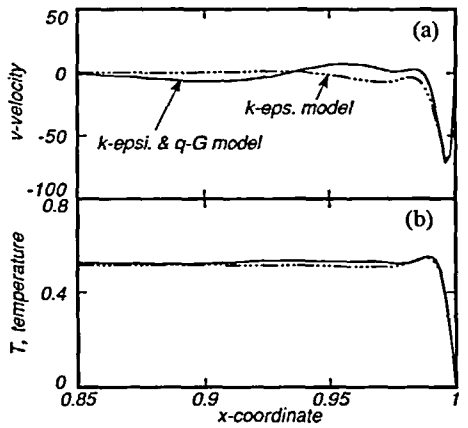

Figure 7 Profiles of (a) the vertical velocity and (b) temperature at the cavity mid-height ($y = 0.5$) near the cooled wall at $x = 1$, predicted by the k–ε and q–G model [model 1] (———) and k–ε model [model 2] (—·····—) for case B

which is extremely difficult to reproduce in laboratory experiments. Realistic thermal boundary conditions for the end surfaces of these heaters/coolers will deviate from those considered in the previous computations due to the presence of heat conduction inside the side wall. A simplified model accounting for the effects of conduction may be constructed by prescribing a small length of a linearly-varying temperature region between the isothermal and uniform heat-flux elements. This will properly simulate the situation in which the wall is made of material having very large thermal capacity and a good conductor of heat, such as metal.

Figure 8 illustrates variations in the local Nusselt number distributions at the side walls with *dl*, the length participating to the interior heat conduction. Case B is considered for the present discussion. The Nusselt number remains at a constant value along the uniform heat-flux surface in $0 \leqslant y \leqslant (1 - dl)/2$. At the left side wall ($x = 0$), sharp *Nu* peaks are observed at the interface of the heating components ($y = 0.5$). The maximum *Nu* is remarkably reduced as *dl* increases. Similar *Nu* gaps are also found at the cooled wall ($x = 1$), albeit in a much less significant manner. It is perceived that the interfacial conduction acts to smooth out the *Nu* discontinuity, as shown clearly in an inset of *Figure 8b*.

Due to the comparatively small size of these conducting lengths, their effects on the *Nu* distributions appear to be localized. The average Nusselt number does not fall more than 2% of the case of $dl = 0$ over the studied range of *dl*. The overall features in the flow and temperature fields are virtually not modified by *dl* (not shown).

Grid dependence of solutions

An additional calculation is performed with a 62 × 63 grid network to assess a grid dependence of the solutions. *Table 3* lists a comparison of the several important flow variables computed using the two mesh systems for Case A. The percentage difference is also indicated, which is seen to be minor. A close-up view of the velocity profile at $y = 0.75$ near the heated wall ($x = 0$)

© Emerald Backfiles 2007

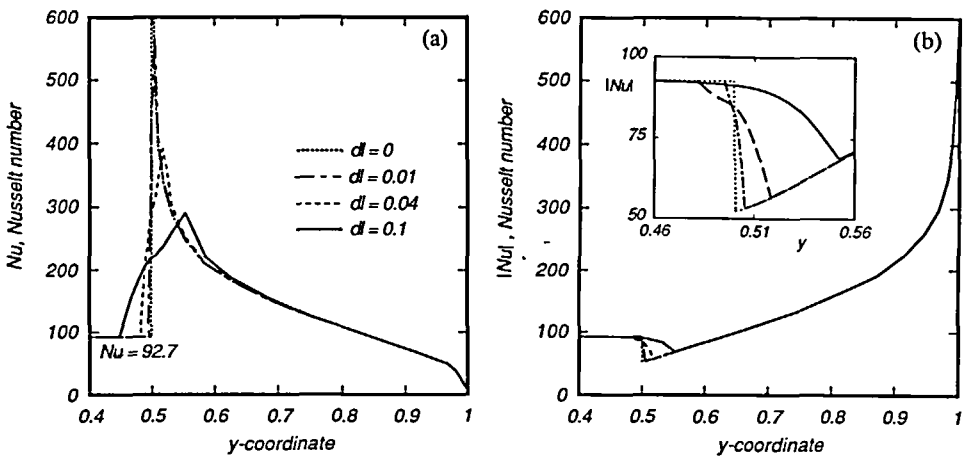

Figure 8 Changes in the local Nusselt number at the side walls with varying length of a conducting surface, dl (case B): (a) at $x = 0$ [maximum Nusselt number (Nu_{max}): 1090 for $dl = 0$, 570 for $dl = 0.01$, 390 for $dl = 0.004$, 290 for $dl = 0.1$], (b) at $x = 1$ [absolute maximum Nusselt number ($|Nu|_{max}$): 52.4 for $dl = 0$, 53.2 for $dl = 0.01$, 56.7 for $dl = 0.04$, 68.7 for $dl = 0.1$]

Table 3 Computed results using 62 × 63 grid points. The figures in brackets indicate the percentage difference between the present predictions and those of 42 × 43 grids (Case A)

u_{max} at $x = 0.5$	v_{max} (x, y)	$\mu_{t,max}$ (x, y)	$\overline{Nu}$
6.42 [1.42%] $y = 0.9885$	98.27 [−0.98%] (0.00332, 0.430)	10.66 [−3.62%] (0.0261, 0.795)	74.3 [−2.11%]

is shown in *Figure 9*. The solution obtained by employing 42 × 43 nodes appears to agree well with that using 62 × 63 grid points. From these results, it may be concluded that the 42 × 43 grids can provide sufficiently accurate predictions for $Ra = 10^{10}$, particularly for mean flow properties.

CONCLUSIONS

A finite difference numerical study is performed on turbulent natural convection in a square cavity using the two-equation models of momentum and heat transfer. For the selected values of $Ra = 10^{10}$ and $Q_{wall} = 0.3$, variations of the field characteristics are investigated by systematically altering the location of the isothermal elements placed on the side walls. The following conclusions may be drawn from the results presented in the previous section.

- In a comparison of the data with those obtained using the conventional high Re k–ε models and a DNS, it was revealed that the present low-Re version of the flow model produced much improved heat transfer results.
- The present turbulent flow calculation procedure for natural convection in enclosures was able to predict successfully the effects of the non-uniform thermal boundary conditions at the side walls. In the demonstrated exemplary results, the regions of the high temperature fluctuations were seen to penetrate into the cavity interior farther than those of velocity fluctuations.

© Emerald Backfiles 2007

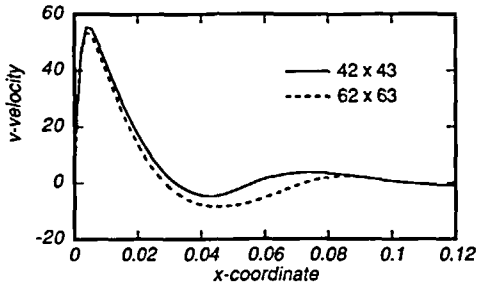

Figure 9 Details of the near wall vertical velocity profiles at $y = 0.75$ computed using 42×43 and 62×63 grid points (case A)

- For the various thermal boundary-conditions studied in the present analysis, the locations of the isothermal surfaces were found to have a measurable impact on the turbulence intensities of flow and heat transfer.
- Heat conduction between the isothermal and constant heat-flux elements of the side walls eliminated unrealistic discontinuities of the heat transfer rate. When the length taking part in the interior heat conduction was small, the global features of the fields were hardly affected.

REFERENCES

1 Markatos, N. C. and Pericleous, K. A. Laminar and turbulent natural convection in an enclosed cavity, *Int. J. Heat Mass Transfer*, **27**, 755–772 (1984)
2 Ozoe, H., Mouri, A., Ohmura, M., Churchill, S. W. and Lior, N. Numerical calculations of laminar and turbulent natural convection in water in rectangular channels heated and cooled isothermally on the opposing vertical walls, *Int. J. Heat Mass Transfer*, **28**, 125–138 (1985)
3 Silva, D. J. and Emery, A. F. A preliminary comparison of the k–ε and algebraic stress models for turbulent heat transfer in a square enclosure, in *Numerical Heat Transfer with Personal Computers and Supercomputing* (Ed. R. K. Shah), *ASME HTD*, **110**, 193–200 (1989)
4 Lankhorst, A. M. Laminar and turbulent natural convection in cavities, *PhD Thesis*, Dept. of Applied Physics, Technical University of Delft, Netherlands (1991)
5 Paolucci, S. Direct numerical simulation of two-dimensional turbulent natural convection in an enclosed cavity, *J. Fluid Mech.*, **215**, 229–262 (1990)
6 Fusegi, T., Hyun, J. M. and Kuwahara, K. Three-dimensional simulations of natural convection in a sidewall-heated cube, *Int. J. Num. Meth. Fluids*, **13**, 857–867 (1991)
7 Ozoe, H., Mouri, A., Hiramatsu, M., Churchill, S. W. and Lior, N. Numerical calculation of three-dimensional turbulent natural convection in a cubical enclosure using a two-equation mode for turbulence, *J. Heat Transfer*, **108**, 806–813 (1986)
8 Lankhorst, A. M. and Hoogendoorn, C. J. Numerical computation of high Rayleigh number natural convection and prediction of hot radiator induced room air motion, *Appl. Sci. Res.*, **47**, 301–322 (1990)
9 Elghobashi, S. E. and Launder, B. E. Turbulent time scales and the dissipation rate of temperature variance in the thermal mixing layer, *Phys. Fluids*, **26**, 2415–2419 (1983)
10 Chung, M. K. and Sung, H. J. Four-equation turbulence model for prediction of the turbulent boundary layer affected by buoyancy force over a flat plate, *Int. J. Heat Mass Transfer*, **27**, 2387–2395 (1984)
11 Nagano, Y. and Kim, C. A two-equation model for heat transport in wall turbulent shear flows, *J. Heat Transfer*, **110**, 583–589 (1988)
12 Nagano, Y., Tagawa, M. and Tsuji, T. A two-equation model for heat transfer taking into account the near-wall limiting behavior of turbulence, *Trans. Japan Soc. Mech. Eng.*, **B 56**, 3087–3093 (1990)
13 Suzuki, N., Matsumoto, A., Nagano, Y. and Tagawa, M. Anisotropy of heat transport and its modeling in homogeneous turbulent flow, *Trans. Japan Soc. Mech. Eng.*, **B 58**, 2565–2570 (1992)
14 Sommer, T. P., So, R. M. C. and Lai, Y. G. A near-wall two-equation model for turbulent heat fluxes, *Int. J. Heat Mass Transfer*, **35**, 3375–3387 (1992)
15 Youseff, M. S., Nagano, Y. and Tagawa, M. A two-equation heat transfer model for predicting turbulent thermal fields under arbitrary wall thermal conditions, *Int. J. Heat Mass Transfer*, **35**, 3095–3104 (1992)

© Emerald Backfiles 2007

16 Patankar, S. V. *Numerical Heat Transfer and Fluid Flow*, Hemisphere, Washington, DC (1980)
17 Leonard, B. P. A stable and accurate convective modelling procedure based on quadratic upstream interpolation, *Comp. Meth. Appl. Mech. Eng.*, **19**, 59–98 (1979)
18 Stone, H. L. Iterative solution of implicit approximations of multi-dimensional partial differential equations, *J. Num. Anal.*, **5**, 530–558 (1968)
19 Anderson, D. A., Tannehill, J. C. and Pletcher, R. H. *Computational Fluid Mechanics and Heat Transfer*, Hemisphere, Washington, DC (1984)
20 de Vahl Davis, G. Natural convection of air in a square cavity: a bench mark numerical solution, *Int. J. Numer. Meth. Fluids*, **3**, 249–264 (1983)
21 Le Quéré, P. Accurate solutions to the square thermally driven cavity at high Rayleigh number, *Computer Fluids*, **20**, 29–41 (1991)
22 Zhang, C. and Sousa, A. C. M. Numerical simulation of turbulent shear flow in an isothermal heat exchanger wall, *J. Fluids Eng.*, **112**, 48–55 (1990)

APPENDIX

Specific expressions for the governing equations:

Stream function equation:

$$\alpha = 0, \qquad \phi = \psi, \qquad \Gamma = 1, \qquad S = -\omega$$

Vorticity equation

$$\alpha = 1, \qquad \phi = \omega, \qquad \Gamma = (1 + \mu_t)/Ra^{1/4},$$

$$S = 2\left[\frac{\partial}{\partial x}\left(\frac{\partial \Gamma}{\partial y}\frac{\partial u}{\partial x}\right) - \frac{\partial}{\partial y}\left(\frac{\partial \Gamma}{\partial x}\frac{\partial v}{\partial y}\right)\right] - \frac{\partial}{\partial x}\left(E\frac{\partial \Gamma}{\partial x}\right) + \frac{\partial}{\partial y}\left(E\frac{\partial \Gamma}{\partial y}\right) - \frac{\sqrt{Ra}}{Pr}\frac{\partial T}{\partial x}$$

where $\mu_t = Ra^{1/4} C_\mu f_\mu k^2/\varepsilon$ with $f_\mu = \exp[-3.4/(1 + 0.02R_t)^2]$, $C_\mu = 0.09$, $R_t = Ra^{1/4}k^2/\varepsilon$, and $E = \partial u/\partial y + \partial v/\partial x$.

Energy equation:

$$\alpha = 1, \qquad \phi = T, \qquad \Gamma = (1 + \lambda_t)/(Ra^{1/4}Pr), \qquad S = 0$$

where $\lambda_t = C_\lambda f_\lambda Ra^{1/2} Pr^2 kq/G$ with $C_\lambda = 0.1$ and $f_\lambda = [1 - \exp(-\sqrt{Pr}\, R_{kx}/26) - \exp(-\sqrt{Pr}\, R_{ky}/26)]^2$, $R_{kx} = Ra^{1/4}\sqrt{k}\,\text{MIN}(x, 1 - x)$ and $R_{ky} = Ra^{1/4}\sqrt{k}\,\text{MIN}(y, 1 - y)$. The symbol MIN$(a, b)$ denotes the smaller of the two arguments, a and b. The friction velocity y^+ contained in the original model[12] is replaced with R_{kx} and R_{ky}, as has been done by Zhang and Sousa[22].

k *equation:*

$$\alpha = 1, \qquad \phi = k, \qquad \Gamma = (1 + \mu_t/Pr_k)/Ra^{1/4}, \qquad S = P_k - \varepsilon + B_k$$

where

$$P_k = \frac{\mu_t}{Ra^{1/4}}\left[2\left(\frac{\partial u}{\partial x}\right)^2 + 2\left(\frac{\partial v}{\partial y}\right)^2 + \left(\frac{\partial u}{\partial y} + \frac{\partial v}{\partial x}\right)^2\right]$$

$$B_k = -\frac{Ra^{1/4}}{Pr}\lambda_t \frac{\partial T}{\partial y}$$

$$Pr_k = 1.0$$

© Emerald Backfiles 2007

ε equation:

$$\alpha = 1, \qquad \phi = \varepsilon, \qquad \Gamma = (1 + \mu_t/Pr_\varepsilon)/Ra^{1/4}, \qquad S = (C_{\varepsilon 1}P_k - C_{\varepsilon 2}f_2\varepsilon + C_{\varepsilon 3}B_k)\cdot(\varepsilon/k)$$

where $C_{\varepsilon 1} = 1.44$, $C_{\varepsilon 2} = 1.9$, $C_{\varepsilon 3} = 0.7$, $Pr_\varepsilon = 1.3$ and $f_2 = 1 - 0.3\exp(-R_t^2)$.

q *equation:*

$$\alpha = 1, \qquad \phi = q, \qquad \Gamma = (1 + \lambda_t/Pr_q)/(Ra^{1/4}Pr), \qquad S = P_q - 2G/(Ra^{1/4}Pr)$$

where

$$P_q = 2\frac{\lambda_t}{Ra^{1/4}Pr}\left[\left(\frac{\partial T}{\partial x}\right)^2 + \left(\frac{\partial T}{\partial y}\right)^2\right]$$

$$Pr_q = 1.0$$

G *equation:*

$$\alpha = 1, \qquad \phi = G, \qquad \Gamma = (1 + \lambda_t/Pr_G)/(Ra^{1/4}Pr)$$

$$S = \frac{G}{q}\left(C_{P1}\frac{P_q}{2} - C_{D1}f_{D1}\frac{G}{Ra^{1/4}Pr}\right) + \frac{G}{k}(C_{P2}P_k - C_{D2}{}^F{}_{D2}\varepsilon)$$

where $C_{P1} = 1.7$, $C_{P2} = 0.64$, $C_{D1} = 2.0$, $C_{D2} = 0.9$, $Pr_G = 1.0$, $f_{D1} = [1 - \exp(-R_{kx}/6) - \exp(-R_{ky}/6)]^2$ and $f_{D2} = (f_{D1}/C_{D2})(C_{\varepsilon 2}f_2 - 1)$, following Nagano *et al.*[12].

© Emerald Backfiles 2007